Aftershocks investigation of 2010 Dec. and 2011 Jan. Rigan earthquakes in the southern Kerman province, SE Iran

Majid Nemati[1, 2]

1) Department of Geology, Faculty of Science and Earthquake Research Center of Shahid Bahonar University of Kerman, P .O .Box 76169133, Pajouhesh Sq., Kerman, Iran.

2) Seismotectonics and Seismology Department of Geological Survey of Iran, Azadi Sq. Tehran, Iran.

* Corresponding Author: nematimajid_1974@uk.ac.ir

Received: 28 April 2014 / Accepted: 11 March 2015 / Published online: 20 March 2015

Abstract

A doublet of earthquakes with magnitudes of 6.5 and 6.2 in M_W scale (Global CMT) on 2010 December 20 and 2011 January 27 respectively struck the area that lies between the Nehbandan and Jiroft fault systems, southeast of Iran. These earthquakes occurred in correspondence of the southwestern termination of the Kahourak right lateral strike slip fault. The focal mechanisms of both the mainshocks and the strongest aftershocks processed with first P motion method confirm the geological observations. They indicate steep dipping coseismic faults for both events, and dominant right lateral and left lateral strike slip motions, if the NE-SW and NW-SE planes are assumed as the active planes for the 2010 and 2011 earthquakes, respectively. A seismogenic zone thickness of 19 km was computed using the relationships between earthquake parameters.

Keywords: Kahourak Fault, Aftershock, Focal Mechanism, Rigan, Eastern Iran.

1– Introduction

The released seismic energy and present-day tectonics in eastern Iran as well as the other seismotectonic provinces (Alborz and Zagros) are determined by the convergence in NE-SW direction between Arabia and Eurasia plates. Seismic hazard assessment in eastern Iran is a significant issue because of the existence of long strike slips faults with mainly ~N-S direction (Bam F., Jiroft F. and also Gowk F.) and sparsely inhabitants near the fault systems. On 2010 December 20 and 2011 January 27 two intra-mountain moderate earthquakes with magnitudes of 6.5 and 6.0 respectively in M_N (Nutli, 1983) scale (Institute of Geophysics, the University of Tehran, IGUT) occurred in the Jebal-e Barez Mountains, SE Iran (Fig. 1). The epicentral area was located ~70 km south of Rigan, a small town in the Kerman province. The events killed four young people who lived in shelters and ramshackle homes in Chah-Ghanbar and villages around, located southwest of Rigan. There is old and valuable seismic information in an ancient country like Iran with a rich documented history. But as the earthquakes affected area is scarcely inhabited, little is known about historical earthquakes, except the 1923 (M_S=5.6) and 1838 (M_S=7.0) earthquakes related to the Kahourak and Nehbandan faults respectively (Ambraseys and Melville, 1982) (Fig. 1). The tremor area has experienced a few instrumental events, the 2003 Bam (M_W=6.6, USGS) and 1998 (M_S=5.3, Harvard CMT) earthquakes with known mechanisms. The Gowk, Sabzevaran, Bam and Jiroft fault zones as well as the Nehbandan (including Kahurak F., southwest termination) fault zones are the seismically active fault systems around the epicentral area. The mentioned faults accommodate the major part of the right lateral motion of southeast Iran. Only the Gowk and Jiroft fault systems from western fault zones are recently active. Some researchers believe that the Bam fault zone is responsible for the 2010 and 2011 events (Ashtari *et al*., 2011).

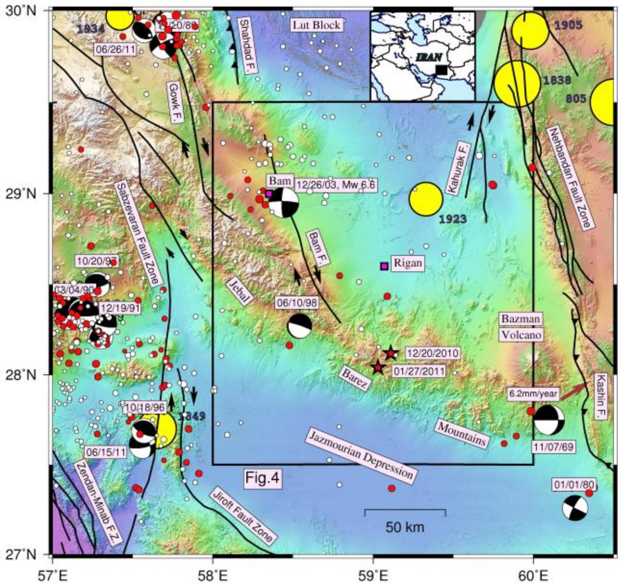

Figure 1) Epicentral area and fault map of southeast Iran. Yellow circles show historical and pre-instrumental earthquakes; red circles represent the Engdahl (Engdahl Catalogue, 2010) relocated events; focal mechanisms are from CMT solution of Harvard University (Harvard Catalogue, 2011); the recent regional microseismicity (IGUT) is characterized by open circles. Brown vector is the GPS velocity at Bazman station. Faults are redrawn from Hessami et al. (2003).

To investigate the post seismic activity and present a coherent picture from seismology, three temporary experimental stations equipped with Güralp CMG-3ESP (Güralp Systems LTD) medium-band seismometers each connected to a DM-24 recorder (GSI) (Table 1) were installed near Rigan a few days after the first shock (Geological Survey of Iran, GSI).

Table 1) GSI stations coordinates.

No.	Station No.	Long.(˚E)	Lat.(˚N)	elevation(m)
1	3797	59.056	28.688	606
2	3768	59.079	28.678	553
3	3798	59.056	28.645	197

Also the telemetric network waveforms of the IGUT permanent stations (SS1 short period sensors connected to Nanometrics digitizers) and mainly CMG-3T broad band sensors of the International Institute of Earthquake Engineering and Seismology of Iran (IIEES) (Tables 2 and 3, respectively) were used as sources of the processed seismological data. In this paper we present the aftershock sequence of the two events, which has not been studied in detail previously, field observations from the main shocks and express how much the seismology confirms both the geology of the earthquakes and the known seismic characteristics of the area.

2– Seismotectonics of southeast Iran

The convergence of Arabia-Eurasia, with a GPS rate of ~21 mm/year (Vernant *et al*., 2004), is absorbed by the Iranian seismotectonic provinces including Eastern Iran. It is responsible for the shortening which dominantly occurs in the Zagros and Alborz. This movement also produces a north-south dextral shearing that accommodates <5 mm/year between Central Iran and the Lut block (Talebian *et al*., 2006), with dominant right lateral strike slip mechanisms of the related earthquakes. The geomorphology of the southeast Iran faults suggests that although little shortening is accommodated across this region, they might still be active, and hence capable of producing earthquakes (Walker and Jackson, 2004). The same authors have also shown that the faults of the Kerman province were active in late Quaternary, therefore capable of producing destructive earthquakes in future. Within the Southeastern Iran, most of the seismic deformation is accommodated along the right lateral large strike slip faults which surround the rigid, flat and aseismic Lut block (Jackson and McKenzie, 1984; Berberian and Yeats, 1999). The Lut block and the Jazmourian Depression are aseismic, while the surrounding areas are characterized by intense seismicity, like the Gowk fault zone (west of Lut) and Nehbandan fault system including Kahurak fault (east of Lut). A part of the Kahourak fault is evident (the one drawn in Fig. 1) and southern part that is inferred and continues to the south is in the study area. Around this block the seismic strain rate decreases during the large historical period (Masson *et al*., 2005). Generally the central Iran experiences no geodetic strain. Also a high seismic strain rate is observed in the northern borders of the Lut block (Masson *et al*., 2005) not at southern part where the Rigan earthquakes occurred.

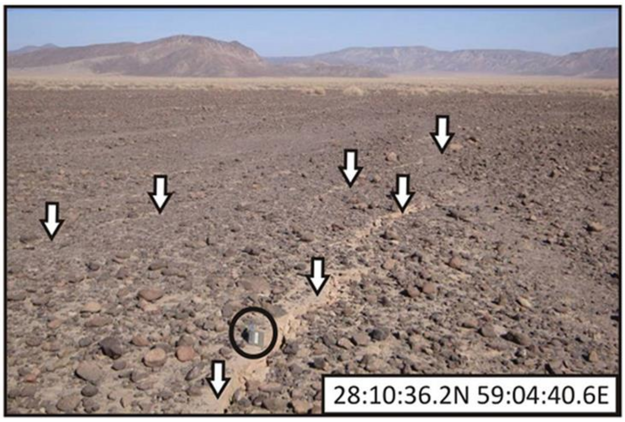

Figure 2) A view of the December 20, 2010 quake rupture, the produced fractures and its extension toward the mountain (Walker et al., 2013).

Figure 3) Co-seismic surface faulting of the 2010 quake. The horizontal and vertical measured displacements are seen in the picture by Walker et al. (2013).

The major part of the seismicity of Iran (Engdahl *et al*., 1998) is closely related to the deformation zone located to the north of central Iran. The study area has only experienced a few historical large pre-instrumental earthquakes. The NNW-SSE trending and SE dipping Gowk fault system, the steep dipping Jiroft, Nehbandan and Bam fault systems and the Kahurak fault compose the seismotectonic framework of the ruptured area (Fig. 1). It consists of a conjugate zone trapped between the southeastern termination of the Kahourak fault and the NW-SE trending fault systems in the Jebale-Barez Mountains. Also the very linear traces of the southern segments of the Kahourak fault zone suggest a steep dipping (Fig. 1). According to Walker *et al*. (2013) the Kahourak fault zone and the Jebal Barez intramountain faults show respectively dextral and sinistral clear evidences of movement from dislocations of streams. The Kahourak fault zone extends and is discontinuously distributed as a right stepping fault through the study area (Meyer and Le Dortz, 2007).

3– Seismicity

The 20 December 2010 earthquake was attributed to a fault zone with an average trend of ~210° and a ~1.3 m right-lateral slip (Walker *et al*., 2013). The 27 January 2011 earthquake was caused by a conjugate left-lateral fault striking ~310°, parallel to the trend of the Jebal-e Barez Mountains, with a left-lateral movement of ~0.6 m. Applying the empirical relations (e.g. Stein and Wysession, 2003; Lee *et al*., 2002) between length of the rupture and magnitude of the 2010 event, it reveals that the surface rupture is not mature. As the 2010 earthquake did not have a mature rupture (Fig. 2) therefore the length of the rupture is adopted from InSAR imagery which is approximately 30km (Walker *et al*., 2013). To obtain the seismic parameters of the 2010 earthquake, we used following information; assuming a shear modulus (μ) of about 3×1011 dyne.cm-2 (Stein and Wysession, 2003; Lee *et al*., 2002), a scalar moment (M_0) adapted from CMT solution (Harvard Catalogue, 2010) equal to 8.38×1025 dyne.cm, approximating the ruptured area by (length of the fault)× (seismogenic zone depth) and the maximum and average dislocations which are measured in the field (average 50cm for horizontal dislocation and 25cm for vertical dislocation; Fig. 3, Walker *et al*., 2013).

Table 2) IGUT stations coordinates.

Sub Network	No.	Station Name	Latitude N (degree)	Longitude E (degree)	Altitude (m)	Sub Network	No.	Station Name	Latitude N (degree)	Longitude E (degree)	Altitude (m)
	1	Afjeh	35.856	51.7125	2750		40	Gharneh	32.4038	52.0418	2020
	2	Damavand	35.5772	52.0322	2546		41	Kolahrood	33.319	51.5787	2280
	3	Firozkooh	35.6415	52.7536	2380		42	Zefreh	32.8956	52.3291	2320
	4	Ghazvin	36.3859	50.2184	2100		43	Pirpir	32.6841	50.8917	2600
	5	Mahdasht	35.6853	50.6675	1150	ISFAHAN	44	Ramesheh	31.8088	52.3815	2000
	6	Qom	34.8424	51.0703	2270		45	Miami	36.3416	60.1017	1684
	7	Razeghan	35.4046	49.929	1950		46	Kardeh	36.7759	59.5146	2245
	8	Sefidab	34.3518	52.2406	948		47	Payeh	36.45	58.996	2100
	9	Tehran	35.7367	51.3817	1462		48	Moghan	36.1082	59.3393	2577
	10	Hasanabad	35.4275	51.3567	1098		49	Mashad	36.3088	59.4703	1150
	11	Varamin	34.9954	51.7273	855	MASHAD	50	Mashad	36.3088	59.4703	1050
	12	Varamin	34.9954	51.7273	855		51	Mouk	29.0461	52.7146	2788
	13	ILPA	35.4761	51.0238	989		52	Pars	29.8419	53.0485	2603
TEHRAN	14	ILPA	35.2128	50.5811	1385		53	Sarvestan	29.3817	53.1133	2688
	15	Marand	38.7133	45.703	1684		54	Kazeroun	29.7796	51.84	2805
	16	Shabestar	38.2833	45.617	2150	SHIRAZ	55	Shiraz	29.6418	52.5133	1595
	17	Tabriz	38.2333	46.147	1650		56	Dehrash	34.6997	46.3867	1434
	18	Azarshahr	37.6783	45.98	2300		57	Komasi	34.1745	47.5102	1502
	19	Heris	38.3183	47.042	2100		58	Ghaleghazi	34.3294	46.5685	2090
	20	Sarab	37.825	47.667	1950		59	Veis	34.5264	46.8496	1135
	21	Bostanabad	37.7	46.892	2100		60	Bozab	34.4696	47.8605	2343
	22	Hashtrud	37.3067	47.263	2805	KERMANSHAH	61	Lien	34.9186	46.9624	2195
TABRIZ	23	Fath-abad	38.0171	46.3944	2222		62	Monand	33.1922	59.6667	2150
	24	Shahmirzad	35.8067	53.2922	2500		63	Kooshah	32.4241	59.0044	2245
	25	Lasjerd	35.3822	52.9589	2195		64	Tejag	32.8965	58.7488	1745
SEMNAN	26	Anjilo	35.4672	53.9144	2135	BIRJAND	65	Dahanechah	32.739	59.868	2277
	27	Qucahn	37.073	58.5394	1320		66	Bandar-abas	27.4489	56.5399	62
	28	Akhelmad	36.6022	58.7566	2508	MINAB	67	Bandar-abas	27.4489	56.5399	62
	29	Emamgholi	37.4155	58.6522	2565	KHORAM ABAD	68	Kafar-mosalman	33.5244	47.8469	_
	30	Sfrayin	37.0538	58	2448		69	Kamar-syah	33.5178	48.3803	_
QUCHAN	31	Shirvan	37.5347	57.7027	1925		70	Ghamsar	33.4564	51.1583	1790
	32	Mehriz	31.3902	54.613	2130		71	Minoodasht	37.2575	55.4069	180
	33	Bafgh	31.5902	55.5673	1485		72	Mahabad	36.7666	45.7167	1344
	34	Sadrabad	31.9136	53.6855	2457	Analog station	73	Brojen	31.908	51.26	2354
YAZD	35	Chekchek	32.2442	54.4073	2030						
	36	Alasht	36.0829	52.8099	2600						
	37	Ghaloghah	36.5024	53.8302	1963						
	38	Kiasar	36.207	53.6837	2167						
SARI	39	Peran	36.2419	52.3381	1333						

We computed a minimum and average value for the seismogenic zone depth ranging 13km - 18.8km respectively. These are strongly supported by the results of Walker *et al*. (2013) (15km) and Tatar *et al*. (2005) (19km) for the Bam area.

To display the seismological behavior and especially the shallow deformation induced by faults of the two earthquakes, we will show the seismicity occurred at the area after both shocks as well as the coseismic activity of the 2011 mainshock. We plotted 117 and 225 aftershocks for the 2010 and 2011 earthquakes respectively. Their waveforms were recorded by the permanent IGUT and IIEES networks with a RMS less than 0.5s. The micro earthquakes were drawn in Figure 4 with respects their M_N magnitudes (IGUT) which vary between 2.5 and 5.0.

Seismic activity is spread over the southern splay of the Kahourak fault with almost two separate clusters concentrated mainly in NW-SE direction for the blue one. The clusters (red and blue clusters in Fig. 4) have weak association with the continuation of the Kahourak fault (2010 coseismic surface rupture) and also with the conjugate direction of the southern part of the Kahourak fault and 2011 coseismic lineament fissures. In this map the location error of the events is more than 5km. Because of the imperfect number and malformed coverage as well as the large spacing of the IGUT and IIEES stations and also because the RMS is not a perfect criterium for event selection, the uncertainty in location might be underestimated and more seismic interpretation based on the events locations in greater details is not reasonable. In other words the seismicity needs to be relocated similar to the relocation which is currently in process as Iranian seismicity clusters in Alborz, eastern Zagros and eastern Iran (Engdahl *et al*., 1996).

The maximum magnitude (M_{Max}) at the mainshocks epicentral area could be estimated 7.2 using the seismic hazard assessment of Tavakoli and Ghafouri-Ashtiani (1999). A maximum 126 $cm.s^{-2}$ peak ground acceleration was recorded at Rigan station (located about 50km northeast of the 2010 earthquake epicenter) by the Building and House Research Center (BHRC) accelerometer network. Moreover, for the mainshocks area it has has been proposed an average 0.2g vertical acceleration (Tavakoli and Ghafouri-Ashtiani, 1999). This is really important and indicates that the area needs to be hazardly reassessed in a detailed scale.

The seismicity depth dispersal seems to be rooted down to 29km. This depth of seismicity is quantitative deep for continental regions, which prevent us giving any interpretation on depth. It comes from the micro earthquakes which have been located by regional networks. The seismogenic zone thickness of the southeastern Iran estimated based on microseismicity depth dispersal located by local seismological networks, extends to maximum 20 km (Tatar *et al*., 2005 and Nemati and Gheitanchi, 2011) in depth.

4– Focal mechanisms

Due to lack of a precise P wave velocity structure for regional works in Iran, we merged the layers widths and averaged out the velocities of the models computed for eastern Iran (e.g. Tatar *et al*., 2005), Zagros (e.g. Yamini-Fard *et al*., 2006) and Alborz (e.g. Nemati *et al*., 2011) seismotectonic provinces as a model for computing focal mechanisms of the events with the regional phases. Computing focal mechanisms of the earthquakes with regional phases using first P motion method is possible if any P phases (Capital P grapheme except pP) is used for polarity picking (Havskov and Ottemöller, 2005; Ottemöller and Havskov, 2012). The location and depth errors of the local earthquakes are more important in comparison to the regional events for focal mechanisms computation. Some researchers (e.g. McKenzie, 1972; Jackson and McKenzie, 1984; Akasheh and Berkmer, 1984; Priestley *et al*., 1994; Ni and Barazangi, 1982) computed focal mechanisms of large Persian earthquakes with Tele-seismic and regional phases using the first P motion method. The take off angle of the regional and Tele-seismic phases are smaller than that the local events ray paths (Stein and

Wysession, 2003). The take off angle of the local phases strongly depends on the depth error of the events. Because of affecting location of the events on their focal mechanism solutions, during the processing, the events #2-4, 6-11, 13-16, 18 and 19 (Fig. 4 and Table 4) fixed on the locations (Walker *et al*., 2013) obtained using hypocentroidal decomposition (HDC) method for multiple event relocation obtained by Jordan and Sverdrup, (1981). We computed first-motion polarity solutions for earthquakes mechanisms recorded with less than 1 polarity error, a RMS less than 0.5s, maximum 5° rotation for nodal planes and M_N>4.0 (IGUT). The remained aftershocks have been relocated (Seisan Software, Havskov J., Ottemöller, 2005) with merging local phases with the readings which could precise the events locations which were not much improved. 22 focal mechanisms were solved for the events with M_N magnitude (IGUT) greater than 4.0 and were drawn according to their magnitudes in Figure 4.

Table 3) IIEES stations coordinates.

No	***station***	***Long.(˚E)***	***Lat.(˚N)***	***elevation(m)***
1	ASAO	50.025	34.548	2217
2	BNDS	56.171	27.399	1500
3	BJRD	57.408	37.7	1337
4	CHTH	51.126	35.908	2350
5	DAMV	51.971	35.63	2520
6	GRMI	47.894	38.81	1300
7	GHIR	52.987	28.286	1200
8	GHVR	51.295	34.48	927
9	KRBR	56.761	29.982	2576
10	MAKU	44.683	39.355	1730
11	MRVT	56.089	37.659	870
12	NASN	52.808	32.799	2379
13	RMKL	49.809	30.982	176
14	SNGE	47.347	35.093	1940
15	SHGR	48.801	32.108	150
16	THKV	50.879	35.916	1795
17	ZHSF	60.775	29.611	1575
18	ZNJK	48.685	36.67	2200
19	AHRM	51.295	28.8641	80
20	BSRN	59.118	31.996	1416
21	GNBJ	58.327	34.3119	2094
22	CHBR	60.6	25.28	125
23	ILAM	46.2	33.62	796
24	MSHD	59.943	36.587	1965
25	MINE	47.6	37.35	1600
26	SHRT	60.295	33.646	837
27	SHRD	56.01	35.99	1264
28	YASJ	51.3	31.1	2186
29	YAZD	54.677	32.455	1000

We split the focal mechanisms (Fig. 4, App.1 and App.2) into two bunches: robust solutions (#2, 4, 7, 8, 10, 11, 12 13, 14, 15, 16, 18, 19 and 21 drawn in heavy colour), selected on the basis of polarity numbers and scattering of the stations in minimum three quadrants, and fair quality (#1, 3, 5, 6, 9, 17, 20 and 22 drawn in light colour). The solutions are in red and blue related to 2010 and 2011 earthquakes respectively. Most of the red solutions, #2, 3, 4 and 5 show right lateral strike slip motion associated with a NE-SW steep north dipping fault plane which has the same direction of the southern continuation of the Kahourak fault. Also the majority of the blue mechanisms, #8, 9, 10, 11, 12, 13, 14, 15, 16, 18, 19 and 22, are well correlated to the conjugate direction of the Kahourak fault and show left-lateral strike-slip motion, if the NW-SE plane is the active plane (Fig. 4). The focal solution #1 belongs to the background seismicity 47 days before strongly activation of the area and displays general right lateral behavior of the Kahourak fault recognized part. Finally, focal mechanisms #6, 17, 20 and 21 had no correspondence with the main fault systems affecting the area.

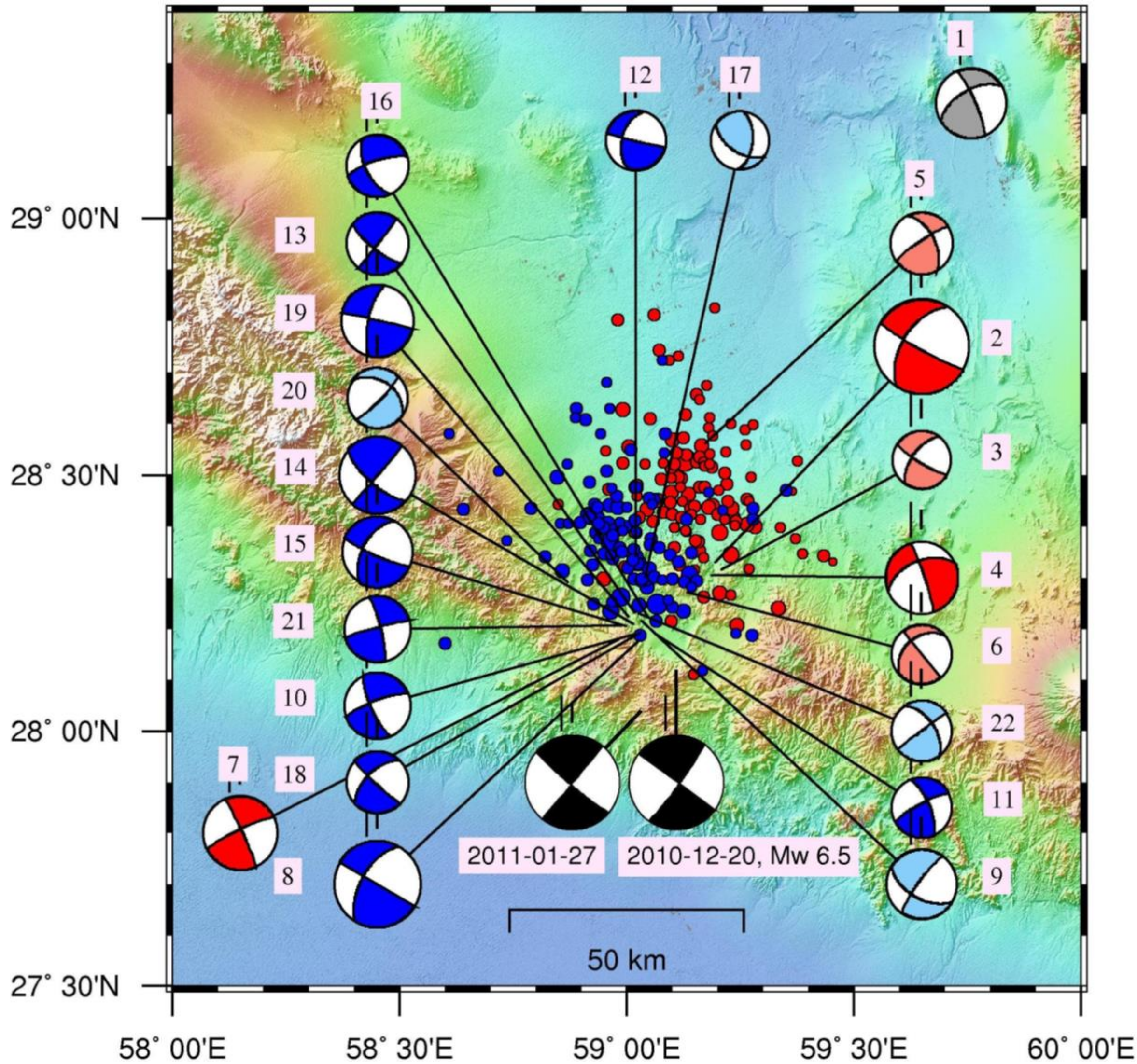

Figure 4. Location of the mainshocks of December 20, 2010 and January 27, 2011 (Harvard catalogue, 2011) and seismicity pattern of the aftershocks (IGUT catalogue, 2011). The black mechanisms indicate CMT solutions for both mainshocks. The red focal mechanisms as well as the red epicenters are related to the 2010/12/20 earthquake and the blue ones are the aftershocks of the 2011/01/27 event (see table1). The focal mechanisms were processed using the first P motion method.

Taking into account the velocity rates recorded at Kerman (16.5 mm/year to the NNE), Bazman (6.2 mm/year to NE - marked in Figure 1) and Jask (14.8 mm/year to the ENE) GPS stations, all reported by Vernant *et al*. (2004), we interpolated the surface movement of the crust in the area affected by the earthquakes, which is estimated to be ~8 mm/year to the north-northeast. The study area is placed in a gradually GPS velocity transition zone which strongly decreases from the northwest (Kerman station) to the southeast (Bazman station). Regarding to the mechanisms of the coseismic faults deduced from this study we could conclude northward motion of the study area (north of the coseismic faults, Figs. 1 and 4) and its consistency with the GPS estimated direction of motion.

Table 4) Earthquake focal mechanisms characteristics processed using first P motion method. The bold location numbers adapted from Walker et al. (2013).

No	Origin Time	Lat.(°N)	Long.(°E)	Depth(km)	M_L	Strike(°)	Dip(°)	Rake(°)
1	2010/11/03 19:56:29.0	29.16	59.66	19	4.8	336.74	80.05	32.68
2	2010/12/20 18:42:02.5	**28.33**	**59.194**	5	6.5	299.1	84.28	-34.59
3	2010/12/20 19:59:49.4	**28.316**	**59.207**	18	4	121.38	80.15	-28.48
4	2010/12/20 22:13:04.3	**28.306**	**59.185**	27.5	5	247.29	50.47	-6.66
5	2011/01/02 15:23:50.1	28.56	59.17	10	4.3	332.02	56.36	10.27
6	2011/01/11 20:05:13.9	**28.272**	**59.132**	5	4.1	320.73	90	50
7	2011/01/27 07:02:06.5	**28.179**	**58.982**	8.4	5.1	335.33	85.79	9.08
8	2011/01/27 08:38:32.7	**28.18**	**59.028**	23.9	6	300	90	30
9	2011/01/27 09:07:54.8	**28.217**	**59.03**	22.6	4.8	120.18	56.36	-10.27
10	2011/01/27 15:01:47.6	**28.189**	**59.015**	3.4	4.6	156.24	74.81	-13.17
11	2011/01/27 21:49:45.8	**28.19**	**59.064**	7	4.2	336.53	69.38	12.55
12	2011/01/27 23:12:57.3	28.34	59.02	19.1	4.1	103.96	88.11	-38.96
13	2011/01/28 04:13:11.2	**28.231**	**59.018**	18	4.3	128.77	75.23	2.66
14	2011/01/28 04:20:42.2	**28.209**	**59.016**	28.4	5.3	131.32	70.08	1.82
15	2011/01/28 05:06:49.5	**28.205**	**59**	20.9	4.9	113.36	81.46	-34.07
16	2011/01/28 06:34:04.1	**28.223**	**59.046**	13.9	4.3	153.05	60.12	-17.03
17	2011/01/28 12:41:28.8	28.3	59.04	22.3	4	124.13	55.81	44.71
18	2011/01/29 00:50:22.8	**28.193**	**59.032**	22.9	4.3	132.85	85.02	-29.62
19	2011/01/29 04:43:19.8	**28.222**	**59.005**	16	5	283.3	88.29	19.93
20	2011/04/11 12:02:15.3	28.29	58.87	29.8	4.2	303.82	41.47	-13.92
21	2011/04/13 03:37:08.2	28.21	58.99	6.2	4.6	345.67	80.61	3.45
22	2011/04/13 03:52:31.6	28.23	59.03	6	4.2	325.08	56.09	2.69

Because the relocated epicenters (Walker *et al.*, 2013) of the first and second mainshocks are situated at the end of related ruptures, in northeast and northwest sides respectively, the 2010 and 2011 ruptures may propagate in a unilateral manner from northeast to southwest and from northwest to southeast directions respectively. This is in consistency with south-southwestward propagation of the Kahourak fault which is perspicuous on satellite pictures (Meyer and LeDortz, 2007).

5– Conclusions

The source of 2010 December 20 and 2011 January 27 earthquakes with M_W magnitudes greater than 6.0 are related to the southern splay of the Kahourak right lateral strike slip fault and its left lateral conjugate system. The focal mechanisms of the mainshocks and greatest aftershocks confirm dominant right lateral and left lateral strike slip motions for 2010 and 2011 coseismic faults if the NE-SW and NW-SE planes are assumed as the active planes respectively. Based on the nodal planes specifications in focal mechanisms, both coseismic faults dip steeply and in these cases there is considerable correspondence between seismology and the geology.

Although the direction of fault outcrop (cracks) of 2011 event is approximately in association with southern extension of the Bam-Baravat fault, mechanism of 2010 and 2011 events and their coseismic ruptures specify the Kahourak fault zone is responsible for the earthquakes.

Using the relations between scalar moment and dislocation of the first quake, a maximum depth of about 19km was computed for the seismogenic zone. This depth, as ruptured depth range, is perfectly supported by the well located seismicity depth reported at this area (Walker *et al*., 2013) and the 2003 Bam earthquake area (Tatar *et al*., 2005) located 80km to the northwest.

The strike slip motions are related to the events of the magnitude greater than 4.0 (focal mechanisms). Therefore we could relate their slip vectors to the active planes and each could be supposed as a major slip on fault plane at depth. Totally the focal mechanisms could imagine depth deformation and crustal behavior of the fault. Considering the fact that surface outcrops (Walker *et al*., 2013) could image geometry different than the fault at depth, in the brittle crust where the rupture propagates. Therefore seismology could basically present a better explanation from coseismic fault behavior especially at depth where the field geology becomes incapable. In this case because of different rheology of the ductile-brittle surface and brittle depth, the depth rupture is wider than the surface.

Acknowledgments:

Hereby I thank the Geological Survey of Iran for preparing field logistics. The author appreciateS Dr. A.A. Mottaghi and Dr. G. Moratti for their comments which help him to improve manuscript.

References:

Akasheh, B., Berckhemer, H. 1984. Focal mechanisms of earthquakes in Iran with special emphasis on small shocks in Tehran region. Neues Jahrbuch für Mineralogie Abhandlungen: 168, 244–255.

Ashtari-Jafari, M. 2011. Teleseismic Source Parameters of the Rigan County Earthquakes and Evidence for a New Earthquake Fault. Pure and Applied Geophysics: DOI 10.1007/s00024-011-0433–9.

Ambraseys, N., Melville, C. 1982. A History of Persian Earthquakes. Cambridge University Press.

Berberian, M., Yeats, R. 1999. Patterns of Historical Earthquake Rupture in the Iranian Plateau. Bulletin of Seismological Society of America: 89, 120–139.

BHRC, Building and House Research Center accelerometer network, 2011, http://www.bhrc.ac.ir.

Engdahl, E. R., Vander, Hilst, R. D., Buland, R.P. 1998. Global teleseismic earthquake relocation with improved travel time sand procedures for depth determination. Bulletin of seismological Society of America: 88, 722-743.

GSI, Geological Survey of Iran, 2011, http://www.gsi.ir.

Guralp systems LTD., 3 Medias House, Calliva Park, Aldermaston, RG7 8EA, UK, www.guralp.com.

IGUT, Institute of Geophysics, the University of Tehran, 2011, http://irsc.ut.ac.ir.

IIEES, International Institute of Earthquake Engineering and Seismology, 2011, http://www.iiees.ac.ir.

Harvard Un. catalogue, Department of Geological Sciences, Centroid Moment Tensor catalogue, 2011, http://www.seismology.harvard.edu/CMTsearch.

Havskov, J., Ottemöller, L. 2005. SEISAN: the earthquake analysis software, version 8.1.

Hessami, K., Jamali, F., Tabassi, H. 2003. Map of Major Active Faults of Iran, Tech. rep., International Institute of Earthquake Engineering and Seismology, Iran, http://www.iiees.ir.

Lee, W. H., Kanamori, H., Jennings, P. C., Kisslinger, C. 2002. International Handbook of Earthquake and Engineering Seismology, IASPEI.

ISC, International Seismological Center, Engdahl Catalougue, 2010, http://www.isc.ac.uk.

Jackson, J. A., Mckenzie, D. 1984. Active tectonics of the Alpine–Himalayan Belt between western Turkey and Pakistan. Geophysical Journal of the Royal Astronomical Society: 77, 185–264.

Jordan, T. H., Sverdrup, K. A. 1981. Teleseismic location techniques and their application to earthquake clusters in the south-central Pacific. Bulletin of the Seismological Society of America: 71, 1105–1130.

Masson, F., Chery, J., Hatzfeld, D., Martinoid, J., Vernant, P., Tavakoli, F., Ghafoury Ashtiani, M. 2005. Seismic versus aseismic deformation in Iran inferred from earthquakes and geodetic data. Geophysical Journal International: 160, 217–226.

McKenzie, D. 1972. Active tectonics of the Mediterranean region. Geophysical Journal of Royal Astrology Society: 30, 109–185.

Meyer, B., LeDortz, K. 2007. Strike-slip kinematics in Central and Eastern Iran: estimating fault slip-rates averaged over the Holocene. Tectonics: 26, doi: 10.1029/2006TC002073.

Nemati, M., Gheitanchi, M. 2011. Analysis of 2005 Dahuieh (Zarand) aftershocks sequence in Kerman province southeast of Iran. journal of Earth and Space Physics, Institute of Geophysics, University of Tehran): 37, 1–9.

Nemati, M., Hatzfeld, D., Gheitanchi, M. R., Sadidkhouy, A., Mirzaei, N. 2011. Seismotectonics and microseismicity of the Astaneh-Firuzkuh faults at eastern Alborz, Iran. Tectonophysics: 506, 11–21.

Ni, J., Barazangi, M. 1986. Seismotectonics of Zagros continental collision zone and a comparison with the Himalayas. Journal of Geophysical Research: 91(8), 8205–8218.

Nuttli, O. W. 1983. Empirical magnitude and spectral scaling relations for mid-plate and plate-margin earthquakes. Tectonophysics: 93, 207–223.

Ottemöller, L., Havskov, J. 2012. SEISAN: The earthquake analysis software, version 9.1.

Stein, S., Wysession, M. 2003. An Introduction to Seismology, Earthquakes and Earth Structure. ISBN 0-86542-078-5.

Priestley, K., Baker, C., Jackson, J. 1994. Implications of earthquake focal mechanism data for the active tectonics of the South Caspian Basin and surrounding regions. Geophysical Journal International: 118, 111–141.

Tavakoli, B., Ghafory-Ashtiani, M. 1999. Seismic Hazard Assesment of Iran. Annali di Geophysica: 42(6), 1013–1021.

Tatar, M., Hatzfeld, D., Moradi, A. S., Paul, A. 2005. The 2003 December 26 Bam earthquake (Iran), M 6.6, aftershock sequence. Geophysical Journal International: 163, 90–105.

Talebian, M., Biggs, J., Bolourchi, M., Copley, A., Ghassemi, A., Ghorashi, M., Hollingsworth, J., Jackson, J., Nissen, E., Oveisi, B., Parsons, B., Priestley, K., Saiidi, A. 2006. The Dahuiyeh (Zarand) earthquake of 2005 February, 22 in central Iran. Geophysical Journal International: 164, 137–148.

USGS, United State Geological Survey, 2011, http://www.neic.usgs.gov.

Vernant, P., Nilforoushan, F., Hatzfeld, D., Abassi, M., Vigny, C., Masson, F., Nankali, H., Martinod, J., Ashtiani, A., Bayer, R., Tavakoli, F., Chéry, J. 2004. Contemporary crustal deformation and plate kinematics in

Middle East constrained by GPS measurements in Iran and northern Oman. Geophysical Journal International: 157, 381–398.

Walker, R. T., Bergman, E. A., Elliott, J. R., Fielding, E. J., Ghods, A-R., Ghoraishi, M., Jackson J., Nemati, M., Oveisi, B., Talebian, M., Walters, R. 2013. The 2010-2011 Konarak (Rigan) earthquake sequence and its implications for distributed deformation and earthquake hazard in southeast Iran. Geophysical Journal International: doi: 10.1093/gji/ggs109.

Walker, R., Jackson, J. 2004. Active tectonics and late Cenozoic strain distribution in central and e astern Iran. Tectonics: 23, doi:10.1029/2003TC001529.

Yamini-Fard, F., Hatzfeld, D., Tatar, M. and Mokhtari, M. 2006. Microseismicity at the intersection between the Kazerun fault and the Main Recent Fault (Zagros-Iran). Geophysical Journal International: 166, 186–196.

Appendices

Appendix 1) Visual characteristics of the computed focal mechanisms.

1

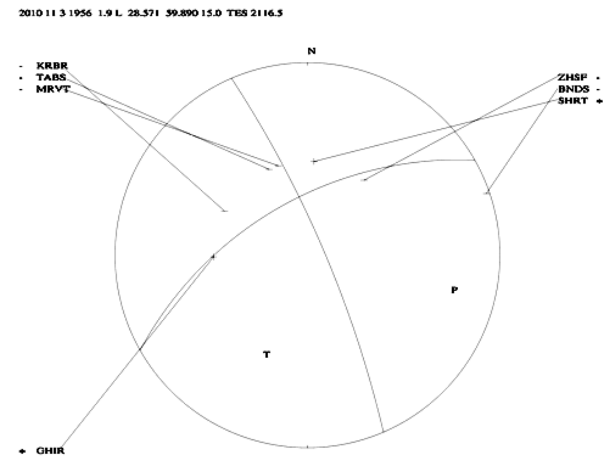

2

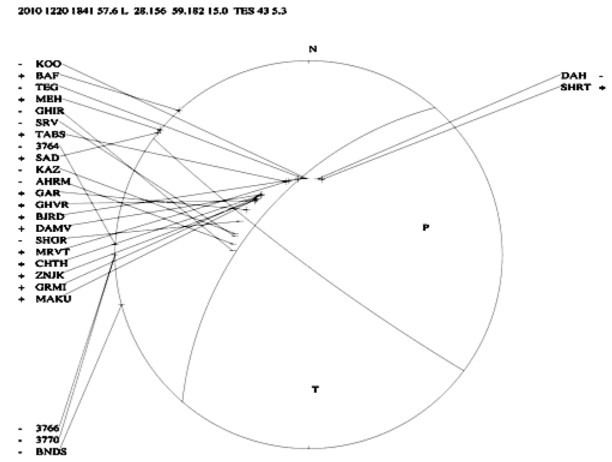

3

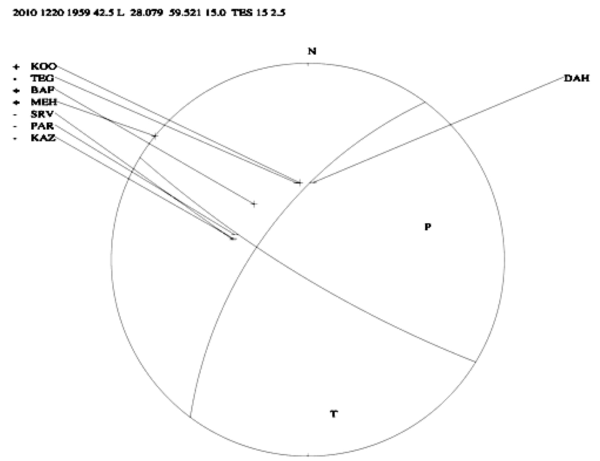

4

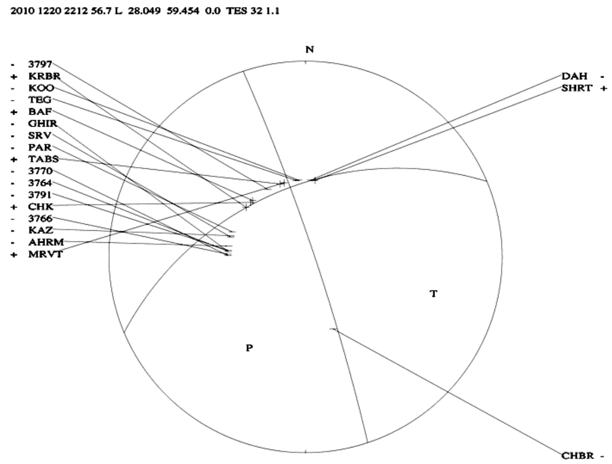

5

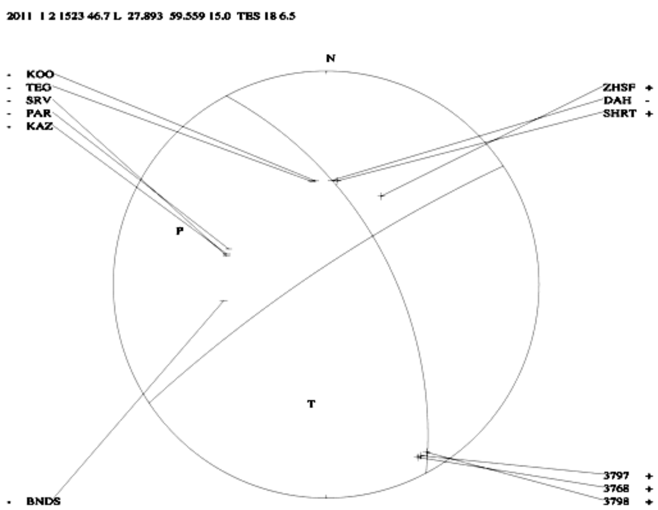

6

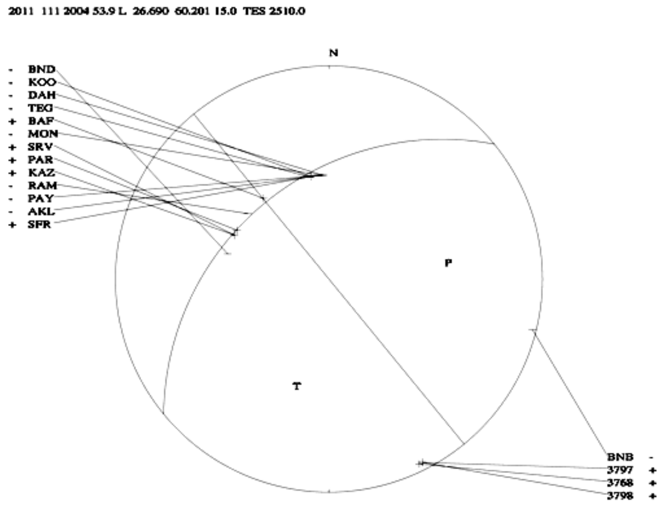

Appendix 1 (Continued)

7

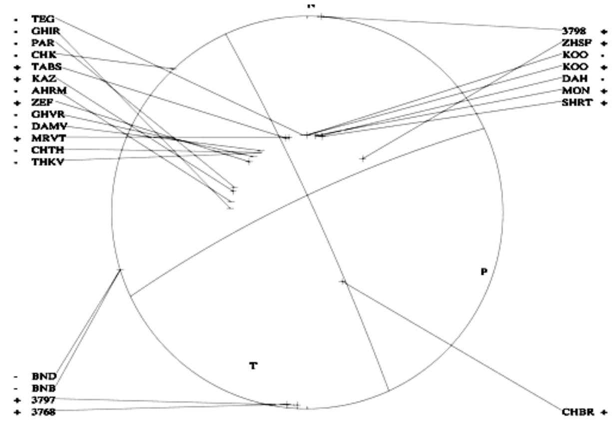

8

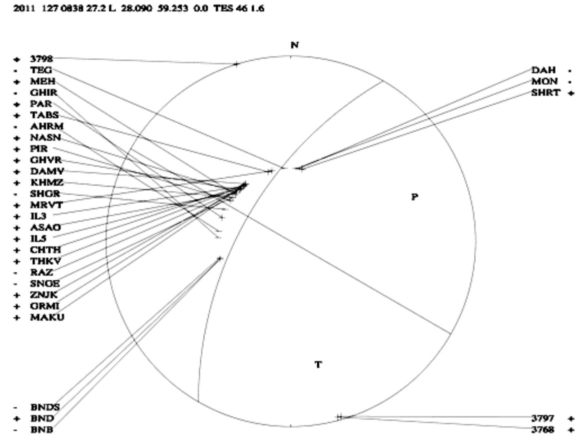

9

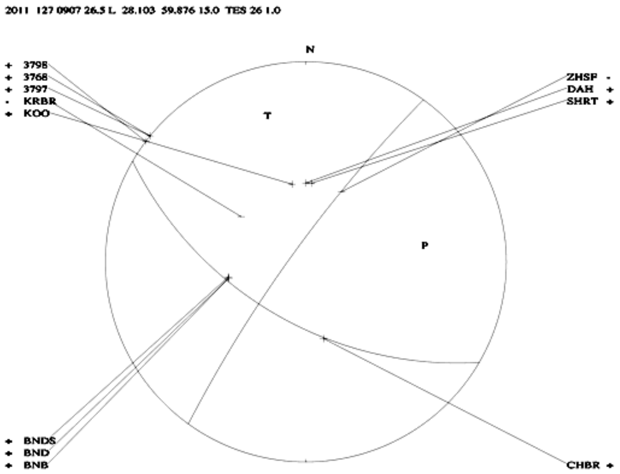

10

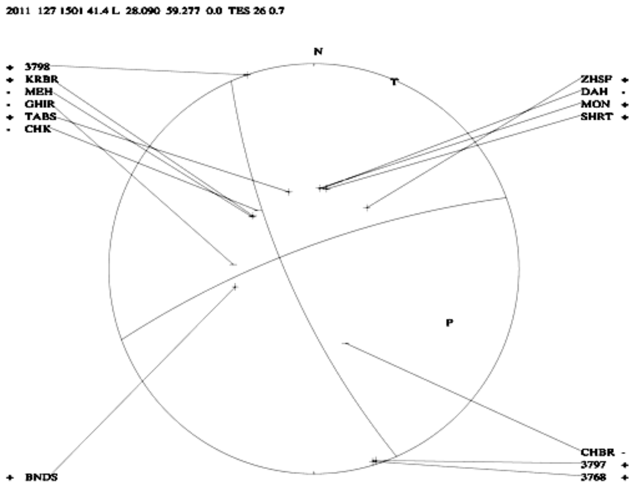

11

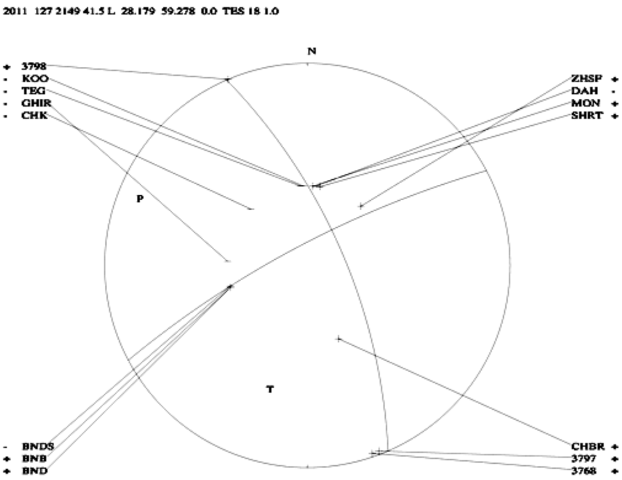

12

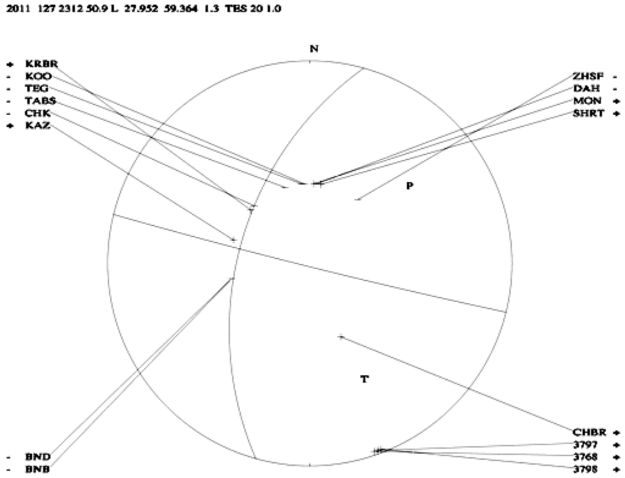

Appendix 1 (Continued)

13

2011 128 0413 4.5 L 28.091 59.275 0.1 TES 25 1.5

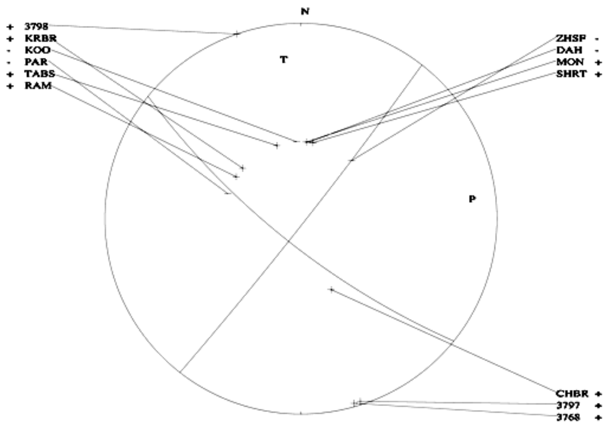

14

2011 128 0420 35.3 L 28.055 59.287 0.0 TES 34 1.4

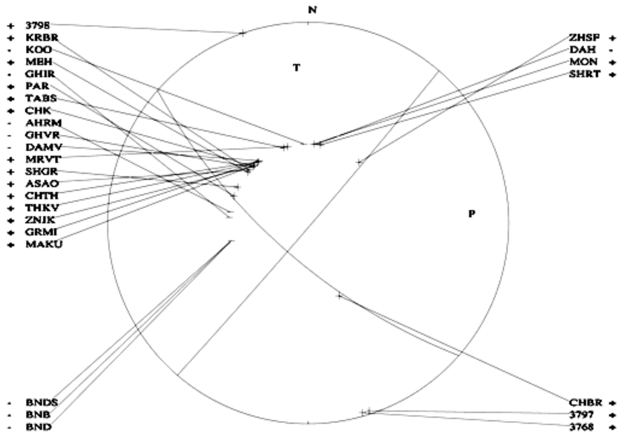

15

2011 128 0506 42.4 L 28.083 59.248 0.0 TES 29 1.2

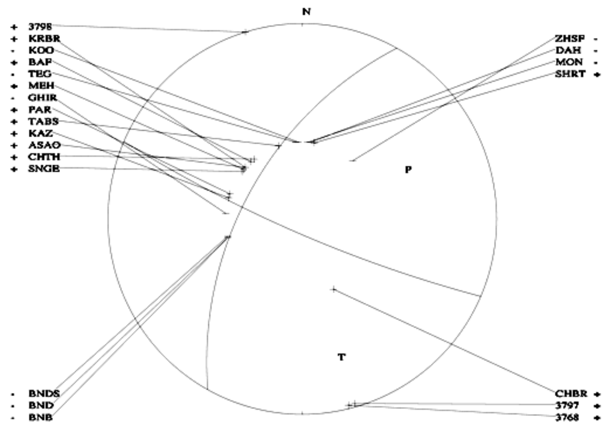

16

2011 128 0633 56.9 L 28.054 59.368 0.1 TES 23 1.3

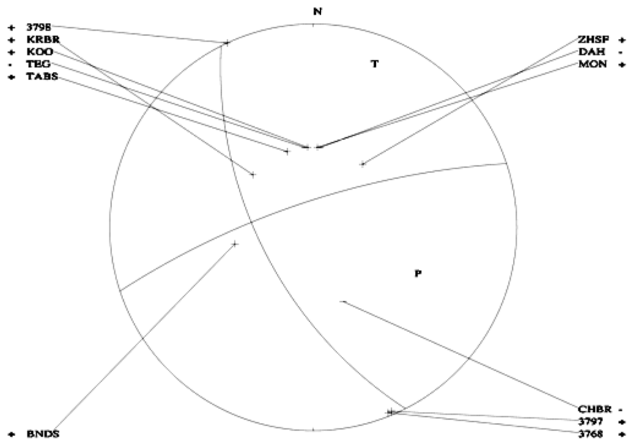

17

2011 128 1241 23.0 L 28.012 59.296 15.0 TES 29 1.6 5.2LTES

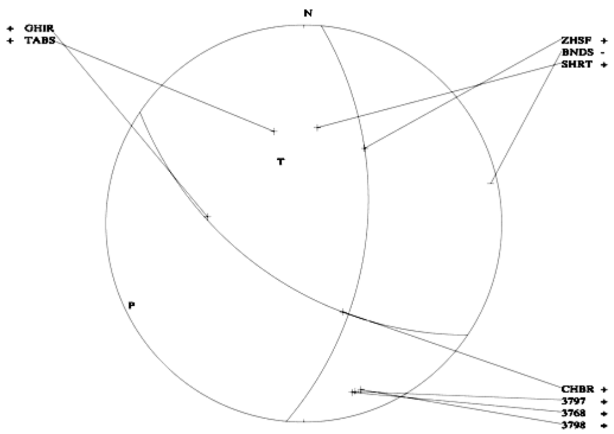

18

2011 129 0050 18.5 L 28.116 59.275 15.0 TES 26 1.1

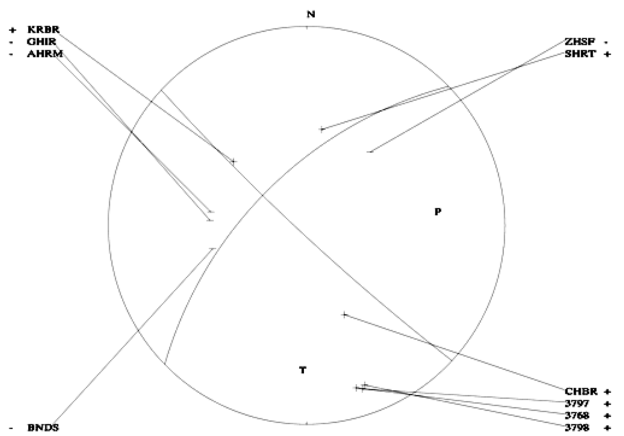

Appendix 1 (Continued)

19

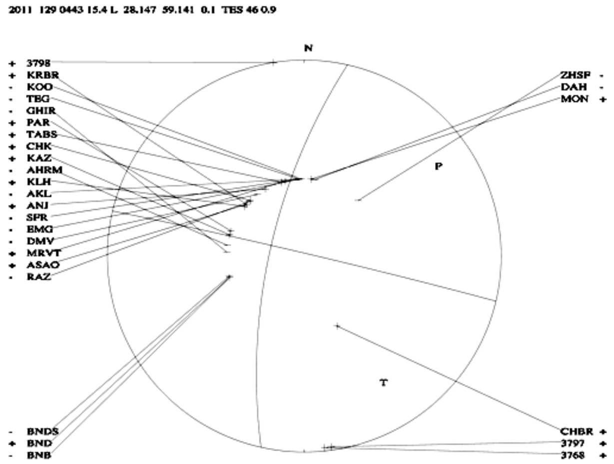

20

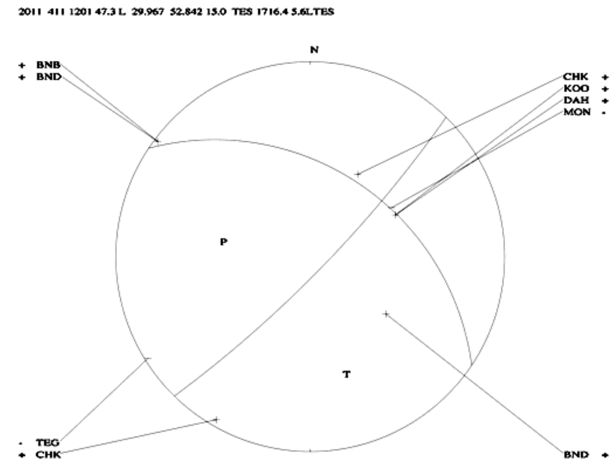

21

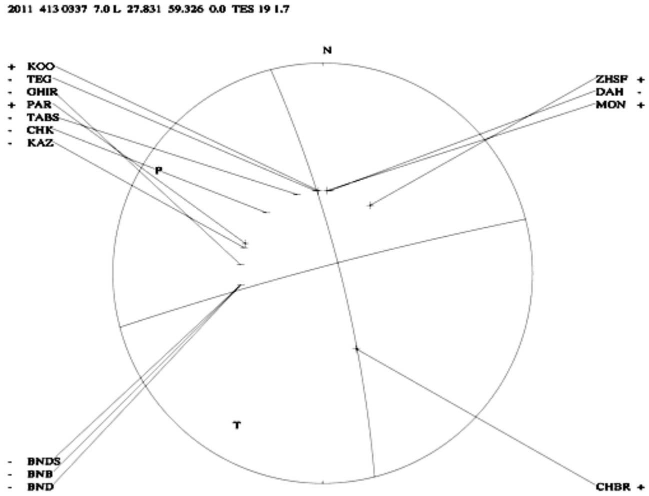

22

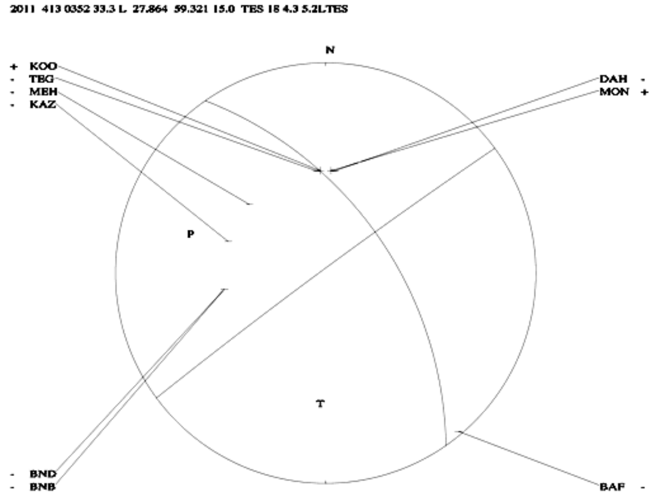

Appendix 2) Some important aftershock waveforms of the computed focal mechanisms (#4, 8 and 19 of the App.1).

1)

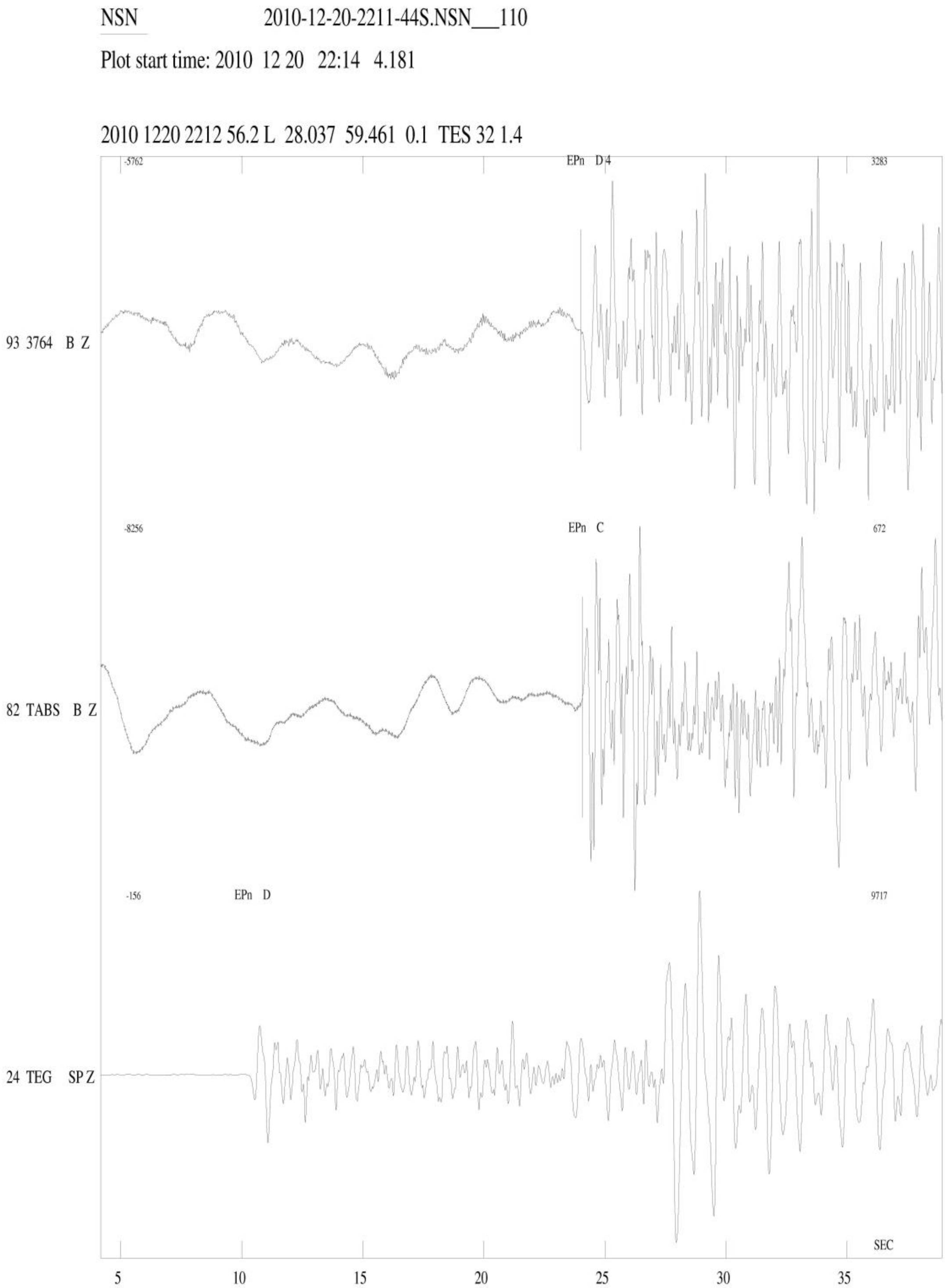

Appendix 2 (Continued)

2)

NSN 2011-01-27-0837-47S.NSN___171

Plot start time: 2011 1 27 8:38 32.940

2011 127 0838 27.0 L 28.084 59.261 0.0 TES 46 1.4

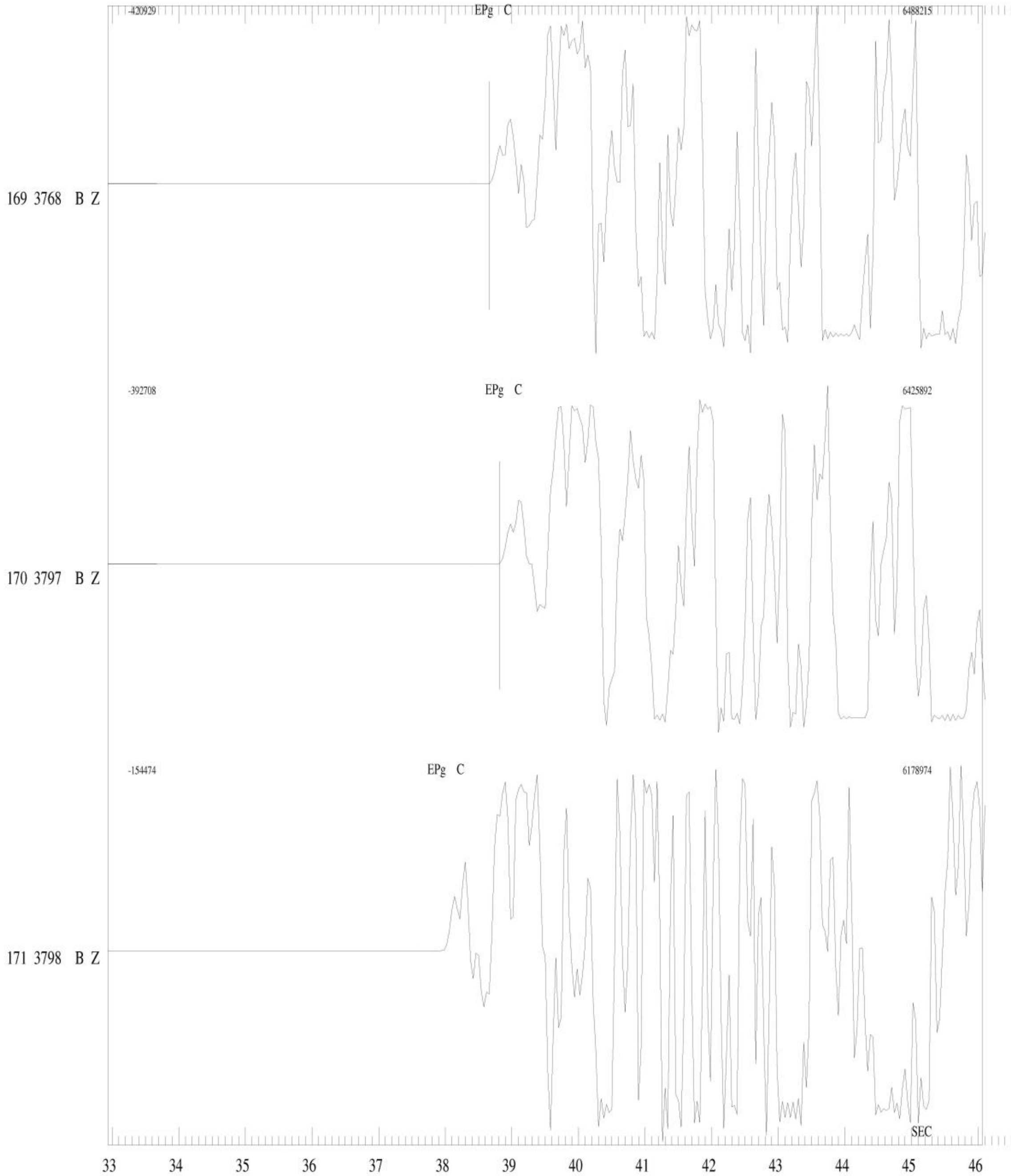

Appendix 2 (Continued)

3)